A neutron diffraction and Mossbauer effect study of the $(FeO_2)_n$ ferromagnetic sheets in antiferromagnetic alpha -$Fe_2(PO_4)O$

1991 J. Phys.: Condens. Matter 3 9597

(http://iopscience.iop.org/0953-8984/3/48/002)

J. Phys.: Condens. Matter 3 (1991) 9597–9612. Printed in the UK

A neutron diffraction and Mössbauer effect study of the $(FeO_2)_n$ ferromagnetic sheets in antiferromagnetic α-$Fe_2(PO_4)O$

M Ijjaali†, B Malaman†, G Venturini†, C Gleitzer†, Gary J Long‡ and F Grandjean§

† Laboratoire de Chimie du Solide Minéral, CNRS URA 518, Université de Nancy I, BP 239, F-54506 Vandoeuvre-les-Nancy Cédex, France

‡ Department of Chemistry, University of Missouri-Rolla, Rolla, MO 65401, USA

§ Institut de Physique B5, Université de Liège, B-4000 Sart-Tilman, Belgium

Received 3 June 1991

Abstract. An unusual feature of the mixed-valence compound α-$Fe_2(PO_4)O$ is the presence of zig-zag chains of face-sharing octahedra running parallel to [010] and containing, alternately, Fe^{2+} and Fe^{3+} ions. These chains form sheets with the composition $(FeO_2)_n$ and, because of the presence of face-sharing octahedra, have a very short Fe^{2+}–Fe^{3+} distance of 2.92 Å. The magnetic properties of α-$Fe_2(PO_4)O$ have been studied by powder neutron diffraction between 4.2 and 280 K and by the Mössbauer effect between 4.2 and 295 K. Below the Néel temperature of 218(3) K, the neutron diffraction data indicate a magnetostriction predominantly along the *c*-axis, magnetic moments at 4.2 K of $3.82(4)\mu_B$ for Fe^{2+} and $4.26(5)\mu_B$ for Fe^{3+} oriented parallel to [010], and the presence of ferromagnetic sheets, containing the zig-zag chains, which are coupled into an overall antiferromagnetic structure. The net antiferromagnetic coupling is the result of a dominant 134° Fe^{3+}–O(1)–Fe^{3+} intersheet superexchange pathway. Ferromagnetic coupling dominates within the sheets and, as a result, the entire magnetic structure avoids any spin frustration. Above 220 K, the Mössbauer effect spectra are paramagnetic and show two quadrupole doublets with hyperfine parameters corresponding to the discrete Fe^{2+} and Fe^{3+} valence states. Below 220 K, the Mössbauer effect spectra show two magnetic components with hyperfine parameters characteristic of discrete Fe^{2+} and Fe^{3+} ions and in agreement with the corresponding paramagnetic values and the magnetic structure.

1. Introduction

The structure of α-$Fe_2(PO_4)O$, which has been prepared and described by Modaressi *et al* [1], has several interesting features which lead to unusual electronic and magnetic properties. Although the PO_4 tetrahedra are isolated, the Fe^{2+} ions occupy octahedra which form edge-shared chains parallel to [010] or the *b*-axis of the orthorhombic unit cell. The Fe^{3+} containing octahedra are connected through face sharing to this chain and alternate with the PO_4 tetrahedra, as shown in figure 1. As a result of the face sharing of the iron containing octahedra, the Fe^{2+}–Fe^{3+} distance is a remarkably short 2.92 Å. Even in the presence of this very short Fe^{2+}–Fe^{3+} distance, the minority-spin electrons are strongly localized on the Fe^{2+} ions, as was demonstrated [2] by the lack of fast

0953-8984/91/489597 + 16 $03.50

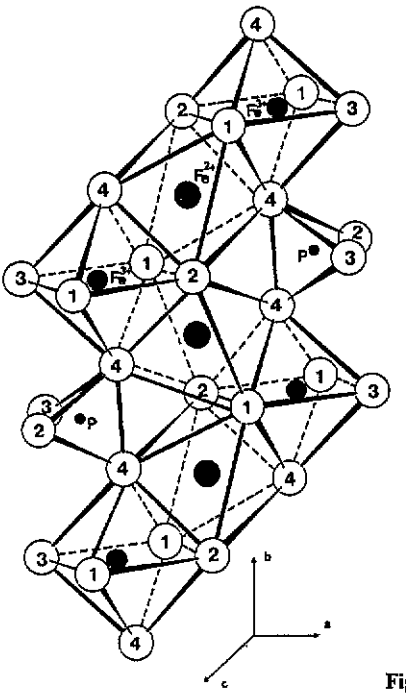

Figure 1. The structure of α-$Fe_2(PO_4)O$.

electron exchange even at 870 K. The strong electron localization apparently results because the Fe^{2+} and Fe^{3+} ions are located on non-equivalent crystallographic sites.

Although a Néel temperature of 220 K has been reported [1] for α-$Fe_2(PO_4)O$, its properties have not been thoroughly investigated below 220 K. The inverse magnetic susceptibility [1] versus temperature for α-$Fe_2(PO_4)O$ shows a minimum at approximately 250 K, a value somewhat higher than the 220 K Néel temperature obtained from the Mössbauer spectra. The antiferromagnetic coupling in α-$Fe_2(PO_4)O$ is believed to result from the rather strong superexchange through the 134° Fe^{3+}–O(1)–Fe^{3+} exchange pathway, which is comparable to that found in various spinels [3].

In general, the octahedral face-shared structure is not favourable for electron delocalization in a mixed-valence material because of the poor 3d orbital overlap. In contrast, the octahedral edge-shared structure is more amenable to electron delocalization in a mixed-valence material because of the better 3d orbital overlap [4–6]. It is interesting to note that α-$Fe_2(PO_4)O$ has a metastable isomeric low-temperature modification [7, 8], β-$Fe_2(PO_4)O$, which has face-sharing octahedra connected by PO_4 tetrahedra [7]. This structure results in an extremely short Fe^{2+}–Fe^{3+} distance of 2.66 Å, which leads to fast electron exchange [9]. Because α-$Fe_2(PO_4)O$ contains discrete valence octahedral face-shared Fe^{2+} and Fe^{3+} ions which are located on non-equivalent crystallographic sites, we have undertaken additional low-temperature studies of its magnetic properties by neutron diffraction and the Mössbauer effect.

2. Experimental details

α-$Fe_2(PO_4)O$ was prepared by a previously described method [1] and characterized by x-ray diffraction and chemical analysis. The neutron diffraction experiments were

Table 1. Room temperature atomic positions in α-$Fe_2(PO_4)O$ structure (from [1]).

	x	*y*	*z*
Fe^{2+}	0	0	0
Fe^{3+}	0.3437(1)	0.75	0.2123(1)
P	0.3784(2)	0.25	0.1296(2)
O(1)	0.0982(4)	0.75	0.1422(5)
O(2)	0.7896(5)	0.75	−0.0051(1)
O(3)	0.0520(5)	0.25	0.4772(5)
O(4)	0.8682(3)	0.4403(3)	0.2478(3)

Table 2. Neutron diffraction reflections and their observed and calculated intensities, magnetic moments, and reliability factor at 4.2 K. $\mu_{Fe^{2+}} = 3.82(4)\mu_B$, $\mu_{Fe^{3+}} = 4.26(5)\mu_B$ and $R = 3.2\%$.

hkl	I_{obs}	I_{calc}
001 100	774	772
010	0	0
101	480	483
110 011	272	279
111	207	227
002 200	107	108
102 201	274	281
012 020 210	555	560
021 120 112 211	1100	1063
121	2196	2203
202	848	860
003 300	395	410
022 212 220	743	754
103	523	417
301	157	176
013 310 122 221	2103	2091
311 113	2867	2492
030	0	0
031 203 302 130	4950	4924
222	697	697

carried out at the Institut Laue Langevin, Grenoble, France. The diffraction patterns were recorded with the one-dimensional curved multidetector D1b instrument with a wavelength of 2.5239 Å. Several patterns were collected within the temperature range 4.2–275 K, namely above and below the Néel ordering temperature of 218(3) K. The Mössbauer spectra were obtained on a Harwell constant acceleration spectrometer which utilized a room temperature Rh matrix Co-57 source and was calibrated at room temperature with natural abundance α-iron foil. The paramagnetic spectra were fitted with symmetric Lorentzian doublets. The magnetic spectra were fitted with a superposition of one sextet assigned to Fe^{3+} and one octet assigned to Fe^{2+}. These magnetic components were calculated [10] from the eigenvalues and eigenvectors of the nuclear ground and excited state Hamiltonians for the combined nuclear quadrupole and magnetic interaction. The accuracy of the hyperfine parameters is ca. 0.002 mm s^{-1} for the

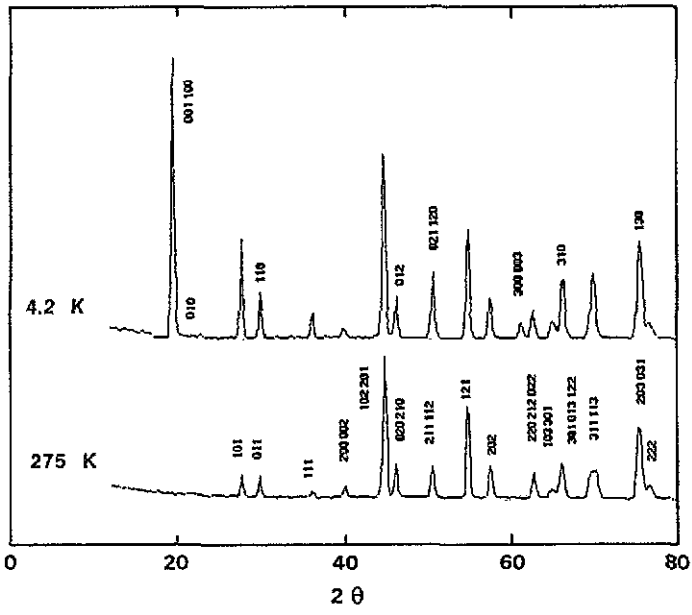

Figure 2. Neutron diffraction patterns of α-$Fe_2(PO_4)O$ obtained at 4.2 and 275 K.

isomer shift, ca. 0.005 mm s^{-1} for the quadrupole interaction, ca. 0.01 mm s^{-1} for the linewidth, better than 2 kOe for the hyperfine field, ca. 2° for θ, and ca. 0.02 for η.

The Wigner–Seitz cell volume was calculated for each crystallographic site in α-$Fe_2(PO_4)O$ by using the program [11] BLOKJE, the room temperature unit cell lattice parameters and atom positions obtained from the single-crystal x-ray study [1], and the ionic radii [12] 0.92, 0.79, 0.31 and 1.28 Å for the Fe^{2+}, Fe^{3+}, P^{5+} and O^{2-} ions, respectively. The cell volumes were also calculated for the antiferromagnetic low-temperature phase by using the room temperature atomic positions [1] and the 4.2 K lattice parameters obtained from the neutron diffraction results reported herein.

3. Magnetic structure

α-$Fe_2(PO_4)O$ crystallizes [1] in the orthorhombic $Pnma$ space group with $a = 7.378(1)$ Å, $b = 6.445(3)$ Å, $c = 7.471(1)$ Å and $Z = 4$. The Fe^{2+} ions are located at a symmetry centre with point symmetry $\bar{1}$ and the Fe^{3+} ions are located on a mirror plane with point symmetry m (tables 1 and 2). As is illustrated in figure 1, the structure may be described as sheets of face-sharing octahedra oriented parallel to [010] and including the PO_4 tetrahedra. These sheets are connected by the O(1) oxygen ions and by the PO_4 tetrahedra.

Two powder neutron diffraction patterns recorded at 275 and 4.2 K are shown in figure 2. The neutron diffraction pattern at 275 K is quite characteristic of nuclear scattering alone. A full refinement is not possible because there are 14 parameters to be determined from 15 independent reflections and 26 observed lines. Nevertheless, by using the scattering lengths [13] $b_{Fe} = 9.54$, $b_P = 5.13$ and $b_O = 5.80 \times 10^{-15}$ m, the nuclear intensities were calculated [14] with the atomic positions determined in the

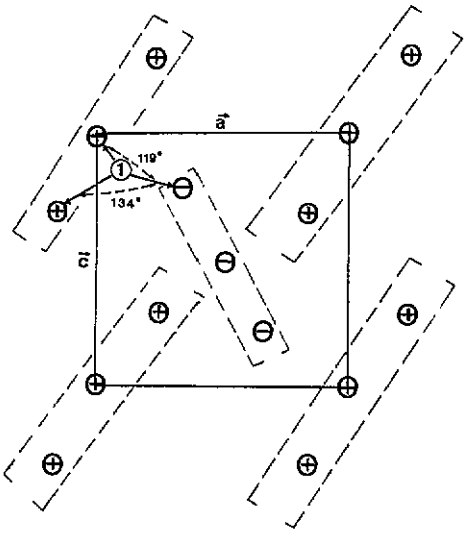

Figure 3. Diagramatic representation of the antiferromagnetic structure and the ferromagnetic sheets in α-$Fe_2(PO_4)O$. In this diagram ⊕ represent iron moments pointing up and ⊖ represent iron moments pointing down. In each block the central iron is Fe^{2+} and the outer irons are Fe^{3+}. The Fe^{2+} ions are at zero and the Fe^{3+} ions are at about ±1.6 Å along *b*.

earlier single-crystal x-ray structure study and yielding a satisfactory reliability factor, $R = 4.1\%$. At 4.2 K, additional lines appear in the neutron diffraction pattern (figure 2) characteristic of an antiferromagnetic ordering, in agreement with the magnetic measurements. All of the observed reflections can be indexed on the basis of the crystal unit cell as $0kl$ with $k + l = 2n + 1$ and $hk0$ with $h = 2n + 1$, i.e. reflections forbidden by the nuclear glide planes *n* and *a* respectively. It must be noted that some of the nuclear reflections have magnetic contributions to their intensity. The refined lattice parameters measured at 4.2 K are 7.404(5), 6.435(5) and 7.443(5) Å for the *a*, *b* and *c* axes, respectively.

Because the structure of α-$Fe_2(PO_4)O$ consists of sheets of octahedra expected to have internal ferromagnetic coupling [1], a model in which these sheets are antiferromagnetically coupled, as shown in figure 3, was used to analyse the low-temperature neutron diffraction pattern. Such a model is in agreement with the observation of the loss of the nuclear glide planes *n* and *a*. Once more, a full refinement is not possible due to the lack of experimental information, 16 variable parameters for 20 independent neutron reflections and 39 observed lines (tables 1 and 2). Therefore, by using the set of nuclear parameters previously defined and the magnetic form factor of iron [15], only the scale factor and the magnetic moments of Fe^{2+} and Fe^{3+} were refined. The best fit to the data was obtained for $\mu_{Fe^{2+}} = 3.82(4)\mu_B$ and $\mu_{Fe^{3+}} = 4.26(5)\mu_B$ with the moments in the [010] direction, with a reliability factor of 3.2% (tables 1 and 2).

The magnetic moment value observed for the Fe^{3+} site is very typical. For instance, it is 4.0 and $4.4\mu_B$ for the two crystallographic Fe^{3+} sites [16] in $Fe_4(PO_4)_3(OH)_3$. However [17], in $Fe_3(PO_4)O_3$, which contains five coordinate Fe^{3+}, the moment is only $3.9\mu_B$. Sherman [18] has carried out a molecular orbital calculation on the $(FeO_6)^{9-}$ cluster and found an effective moment of $4.69\mu_B$. The magnetic moment value observed for the Fe^{2+} site is in the range expected and agrees rather well with the value of $4.1\mu_B$ found for the isolated discrete valence Fe^{2+} in ilvaïte [5].

The thermal dependence of the magnetic intensity measured at various temperatures between 275 and 4.2 K yields a classical thermal variation of the iron magnetic moments

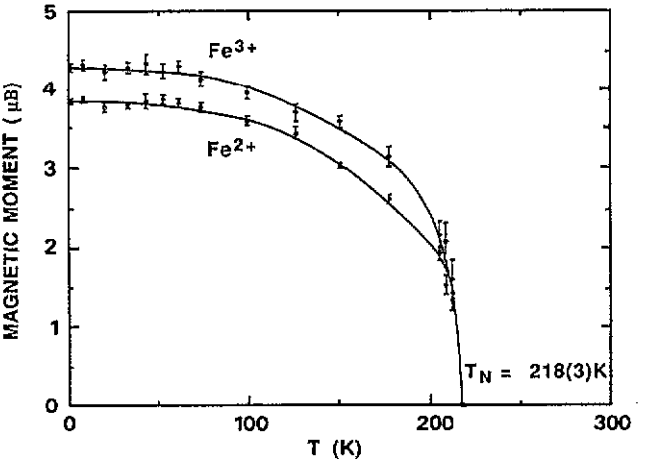

Figure 4. The temperature dependence of the Fe^{2+} and Fe^{3+} magnetic moments in α-$Fe_2(PO_4)O$.

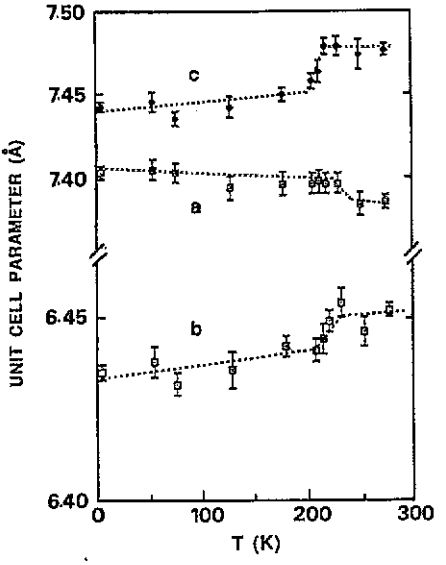

Figure 5. The temperature dependence of the lattice parameters of α-$Fe_2(PO_4)O$.

(see figure 4) and an ordering temperature of 218(3) K; a value which is in fair agreement with the Mössbauer spectroscopy measurements [1].

The temperature dependence of the unit cell parameters is shown in figure 5. An abrupt change in the *b* and *c* lattice parameters and a less pronounced change in the *a* lattice parameter are observed at the Néel temperature. The antiferromagnetic transition is thus accompanied by a rather anisotropic magnetostrictive effect which is fairly common in antiferromagnetic compounds [19]. It should be noted that the major variation of the lattice parameters occurs between 150 and 220 K.

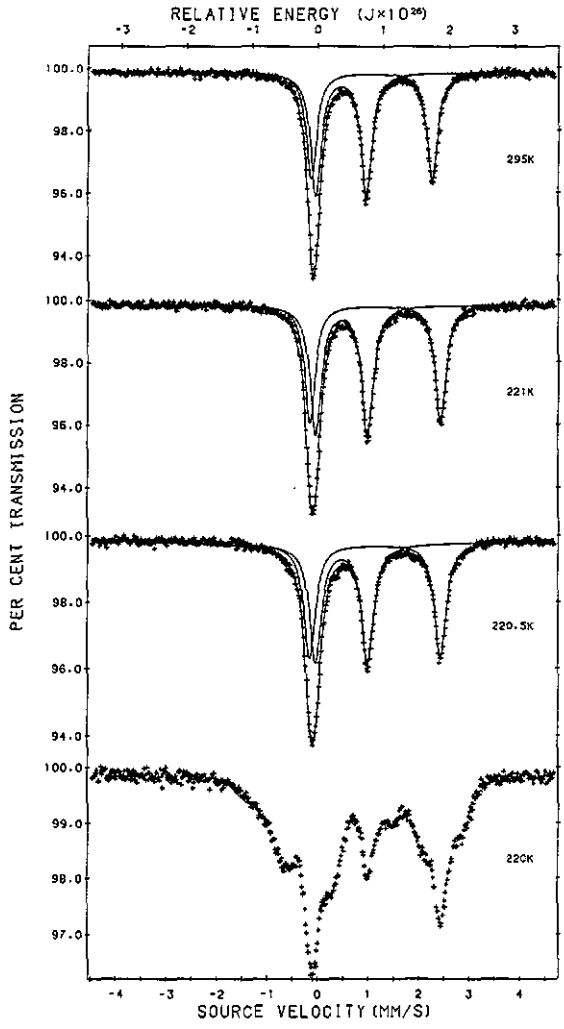

Figure 6. The Mössbauer spectra of α-$Fe_2(PO_4)O$ obtained between 220 and 295 K.

4. Mössbauer spectra

The Mössbauer effect spectra have been measured from 4.2 to 295 K. Between 221 and 295 K, the spectrum consists of two quadrupole doublets as shown in figure 6. Upon slow cooling below 221 K the first indication of ordering is observed at 220.5 K as a broadening and the appearance of shoulders. At 220 K, as shown in figure 6, there is a clear indication of magnetic ordering.

It is possible to obtain two different quadrupole doublet fits [1, 2] of the paramagnetic spectra because of the overlap of the two doublets at approximately zero mm s^{-1}. Both doublet combinations have been tried and cannot be distinguished on the basis of the misfit. The temperature dependence of the isomer shifts between 295 and 873 K, was used by Iraldi *et al* [2] to choose the coupling (1,3) and (2,4) of the four lines. Because

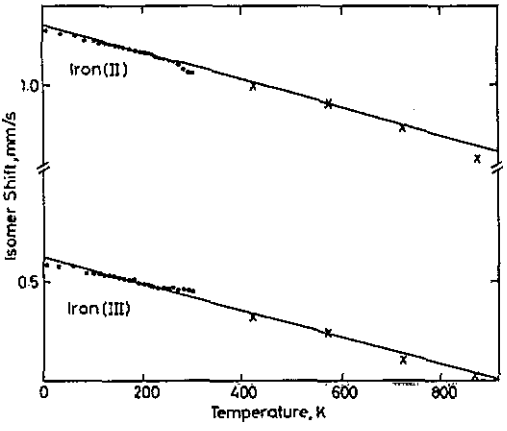

Figure 7. The temperature dependence of the isomer shifts for the Fe^{2+} and Fe^{3+} sites in α-$Fe_2(PO_4)O$. The × data points are from [2].

we have obtained a large number of spectra from 4.2 to 295 K, the temperature dependence of all hyperfine parameters may be followed in detail, in both the magnetic and paramagnetic regions. We expect a smooth temperature dependence of the isomer shifts in each region, in agreement with the second-order Doppler shift [20, 21]. A small discontinuity in the isomer shifts at the Néel temperature would not be abnormal, in view of the lattice parameter variation observed in the neutron diffraction measurements. The relative lattice contraction of ca. 0.7% below the Néel temperature would lead to an increase in electron density of about 0.7% which, if entirely converted into an increase in the 4s electron density, would lead [22] to a decrease of ca. 0.005 mm s^{-1} in both isomer shifts. Such a small decrease would be extremely difficult to observe and we thus do not expect to see any discontinuity in the temperature dependence of the isomer shifts at the Néel temperature. As discussed below, there is no ambiguity in the values of the isomer shifts in the magnetic spectra. If the coupling (1,4) and (2,3) of the four lines of the paramagnetic spectra in figure 6 is chosen, a smooth temperature dependence of the isomer shifts, as shown in figure 7, is observed through the antiferromagnetic transition. If the alternate (1,3) and (2,4) coupling is chosen, a discontinuity of +0.05 mm s^{-1} for the Fe^{2+} site and −0.05 mm s^{-1} for the Fe^{3+} site is observed with increasing temperature at the magnetic transition. Such large discontinuities are not realistic and their different signs are an artefact of the incorrect coupling of the lines. Hence, the fits shown in figure 6 result from the (1,4) and (2,3) coupling of the lines, and the corresponding hyperfine parameters are given in table 3. The temperature dependence of the quadrupole interactions from 4.2 to 873 K will be discussed below.

The isomer shift for the inner doublet is very characteristic of high-spin Fe^{3+} in a pseudo-octahedral oxygen environment [23] in which the Fe^{3+} is bonded to oxygen ions which are also part of a PO_4 tetrahedron. Indeed, the observed room temperature isomer shift of 0.466 mm s^{-1} agrees well with the value of 0.44 mm s^{-1}, the average of the isomer shifts for Fe^{3+} in seven compounds [23] in which the Fe^{3+} is bonded to a PO_4 group through an oxygen. However, the quadrupole interaction for the Fe^{3+} is rather large because of its rather distorted octahedral environment [1]. The isomer shift and the quadrupole splitting of the second doublet are very characteristic of high-spin Fe^{2+} in a distorted octahedral oxygen environment [24]. At this point it is useful to introduce the 295 K Wigner–Seitz cell volume for the two iron sites in α-$Fe_2(PO_4)O$. The cell

Table 3. Mössbauer effect hyperfine parameters for α-$Fe_2(PO_4)O$ in the paramagnetic phase. The isomer shift, δ, is reported relative to room temperature natural abundance α-iron foil.

	Iron (III)				Iron (II)			
T (K)	δ (mm s^{-1})	ΔE_Q (mm s^{-1})	Γ (mm s^{-1})	Area (%)	δ (mm s^{-1})	ΔE_Q (mm s^{-1})	Γ (mm s^{-1})	Area (%)
220.5	0.487	1.029	0.28	51.1	1.148	2.583	0.28	48.9
221	0.483	1.025	0.27	53.6	1.147	2.584	0.25	46.4
222	0.484	1.026	0.26	53.8	1.146	2.581	0.25	46.2
225	0.479	1.018	0.26	52.4	1.144	2.579	0.26	47.6
230	0.477	1.019	0.27	53.1	1.138	2.564	0.27	46.9
240	0.474	1.020	0.26	52.8	1.131	2.532	0.26	46.2
250	0.473	1.016	0.27	53.5	1.121	2.515	0.27	46.5
260	0.475	1.009	0.28	53.1	1.109	2.497	0.28	46.9
270	0.467	1.003	0.27	53.1	1.099	2.461	0.27	46.9
280	0.469	0.980	0.30	52.9	1.079	2.445	0.30	47.1
290	0.467	0.973	0.30	52.7	1.062	2.407	0.30	47.3
295	0.464	0.981	0.28	52.8	1.060	2.386	0.28	47.2
315	0.469	0.967	0.28	54.4	1.019	2.320	0.26	45.6
423[a]	0.326	1.100	0.26	48.3	0.995	1.890	0.24	51.7
573[a]	0.245	1.180	0.27	50.4	0.905	1.560	0.30	49.6
723[a]	0.105	1.165	0.32	50.4	0.795	1.170	0.33	49.6
873[a]	0.025	1.180	0.33	52.3	0.635	0.980	0.36	47.7

[a] Data from [2].

volume is 5.94 $Å^3$ for the Fe^{2+} site and 3.59 $Å^3$ for the Fe^{3+} site. The cell volumes are 0.25, 15.06, 15.44, 17.27 and 15.63 $Å^3$ for the P, O(1), O(2), O(3) and O(4) sites, respectively. The cell volume for the Fe^{2+} site is very similar to the 5.91 $Å^3$ value found [23] for the divalent Fe(3) in $Fe_9(PO_4)O_8$. Hence it is not surprising to find that the Fe^{2+} sites both have the same 295 K isomer shift of 1.07 mm s^{-1}. A similar comparison of the Fe^{3+} sites in α-$Fe_2(PO_4)O$ and $Fe_9(PO_4)O_8$ is less useful because the trivalent Fe(2) in $Fe_9(PO_4)O_8$ is not bonded to a PO_4 group. However, the Wigner–Seitz cell volume of 3.59 $Å^3$ for the Fe^{3+} in α-$Fe_2(PO_4)O$ is substantially smaller than the 4.10 $Å^3$ value found [21] for the trivalent iron in $Fe_9(PO_4)O_8$.

The areas of the two quadrupole doublets in α-$Fe_2(PO_4)O$ are not in a 1:1 ratio but on average the Fe^{3+} doublet contains 53.8% of the Mössbauer spectral absorption area. This indicates that the Fe^{3+} site has a slightly higher recoil-free fraction than does the Fe^{2+} site, in agreement with the smaller thermal parameter found [1] for the Fe^{3+}. This also agrees with the Wigner–Seitz cell volume for the two iron sites, especially when the ratio of the Wigner–Seitz cell volume is compared to the volume of the spherical ion of the radius used in the cell calculation. The ratios are 1.74 for the Fe^{3+} site and 1.82 for the Fe^{2+} site. It would appear that the Fe^{2+} has more volume for recoil and hence a smaller recoil-free fraction. The opposite is the case in $Fe_9(PO_4)O_8$ in which the trivalent Fe(2) site has the largest ratio and the smallest recoil-free fraction [23].

At 220 K, the Mössbauer spectrum of α-$Fe_2(PO_4)O$ shows evidence of long-range magnetic ordering, see figure 6, and from 4.2 to 217.5 K the Mössbauer spectra clearly show evidence for two magnetic components, as is illustrated in figure 8 at several different temperatures. Modaressi *et al* [1], have reported the Mössbauer spectrum of α-$Fe_2(PO_4)O$ at 100 K, but did not fully analyse its hyperfine parameters. More

specifically, they did not relate the Fe^{3+} quadrupole shift in the magnetic spectrum to the quadrupole splitting in the paramagnetic spectrum. In this work, by solving the ground and excited state Hamiltonians [10], a complete analysis of the magnetic spectra is possible and the resulting hyperfine parameters are given in table 4. This analysis for the Fe^{2+} site was based on the values reported by Modaressi *et al* [1]. We used their two sets of parameters with ϕ, the angle between the projection of the hyperfine field onto the plane normal to the principal axis of the electric field gradient, equal to zero in order to avoid complex terms in the Hamiltonians [10]. The parameters given in table 4 provide a better fit to the experimental data than the alternate set reported by Modaressi *et al* [1].

The three parameters describing the quadrupole perturbation, η, the asymmetry parameter, θ, the angle between the principal axis of the electric field gradient and the hyperfine field, and $eQV_{zz}/2$, the quadrupole interaction for the Fe^{3+} site, are strongly correlated. Hence in the fits shown in figure 8, we have kept the quadrupole interaction constant and equal to -1.12 mm s^{-1}, assuming that any temperature dependence of the quadrupole perturbation would be reflected in the temperature dependence of η and θ. For an Fe^{3+} ion, the temperature dependence of the quadrupole perturbation is expected to be due to the temperature dependence of the lattice parameters shown in figure 5. Hence, the quadrupole interaction is expected to be nearly temperature independent between 4.2 and 180 K and to perhaps show some variation above 180 K. Figure 9 shows the temperature dependence between 4.2 and 295 K of the quadrupole splitting

$$\Delta E_Q = (eQV_{zz}/2)(1 + \eta^2/3)^{1/2}$$

for the Fe^{3+} site. The results are in good agreement with the temperature dependence of the lattice parameters shown in figure 5.

For the Fe^{2+} site, the three parameters describing the quadrupole perturbation, η, θ and $eQV_{zz}/2$, are less strongly correlated because of the presence of the seventh and eighth lines in the spectra. Hence, for the Fe^{2+} site all three parameters were adjusted. Between 4.2 and 140 K, they were found to be independent of temperature, in agreement with the temperature independence of the lattice parameters. Figure 10 shows the temperature dependence of the quadrupole splitting, ΔE_Q, for the Fe^{2+} site, between 4.2 and 873 K. The data points at 423 K and above are from [2] and correspond to the coupling (1,3) and (2,4) of the four lines in the paramagnetic spectra. The temperature dependence of ΔE_Q for the Fe^{2+} site, between 4.2 and 873 K, is consistent with the model proposed by Ingalls [25] and given by the expression

$$\Delta E_Q(T) = \Delta E_Q(0)\{[1 - \exp(-\Delta E/kT)]/[1 + 2\exp(-\Delta E/kT)]\} \qquad (1)$$

where $\Delta E_Q(0)$ is the quadrupole splitting at 0 K, and ΔE is the low-symmetry crystal field splitting of the t_{2g} orbitals, which would be degenerate in a perfectly octahedral environment. The full curve in figure 10 corresponds to a $\Delta E_Q(0)$ of 2.79 mm s^{-1} and a ΔE value of 850 K which is equivalent to 590 cm^{-1}. The ΔE value is in excellent agreement with the earlier [2] estimation of 600 ± 40 cm^{-1}. The asymmetry parameter, η, for the Fe^{2+} site is constant from 4.2 to 160 K and decreases above 160 K, in agreement with the temperature dependence of the lattice parameters. Because the values of ΔE_Q measured for the Fe^{2+} site above room temperature are on the same curve as the values measured below room temperature, we conclude that the low-velocity lines of the two doublets must cross each other between 295 and 423 K.

The temperature dependence of the Mössbauer effect hyperfine fields for the Fe^{2+} and Fe^{3+} sites in α-$Fe_2(PO_4)O$ is shown in figure 11. The Mössbauer effect results

Table 4. Mössbauer effect hyperfine parameters for α-$Fe_2(PO_4)O$ in the antiferromagnetic phase. Data obtained upon warming except as indicated. The isomer shift, δ, is reported relative to room temperature natural abundance α-iron foil. The Fe^{3+} quadrupole interaction, $eQV_{zz}/2$, was constrained to the value of -1.12 mm s^{-1}.

	Iron (III)					Iron (II)					
T (K)	δ (mm s^{-1})	H (kOe)	θ (deg)	η	Γ (mm s^{-1})	δ (mm s^{-1})	$eQV_{zz}/2$ (mm s^{-1})	H (kOe)	θ (deg)	η	Γ (mm s^{-1})
4.2	0.591	500	82	0.39	0.28	1.274	2.706	241	66	0.43	0.28
30	0.586	500	78	0.34	0.28	1.252	2.694	240	66	0.43	0.28
60	0.586	494	80	0.36	0.28	1.250	2.654	237	66	0.43	0.28
85	0.546	490	79	0.36	0.33	1.224	2.700	233	66	0.43	0.32
100	0.542	483	80	0.35	0.34	1.223	2.700	228	66	0.43	0.34
110	0.538	477	81	0.39	0.32	1.213	2.700	222	66	0.43	0.32
120	0.533	468	82	0.38	0.31	1.211	2.700	217	66	0.43	0.32
130	0.530	461	79	0.35	0.28	1.203	2.700	212	66	0.43	0.28
140	0.528	452	77	0.31	0.32	1.200	2.700	205	66	0.43	0.32
150	0.519	443	76	0.31	0.30	1.192	2.680	201	66	0.43	0.30
160	0.517	426	80	0.32	0.32	1.192	2.650	192	66	0.42	0.32
170	0.511	418	82	0.37	0.32	1.184	2.644	187	66	0.42	0.32
180	0.511	394	81	0.36	0.32	1.176	2.610	174	66	0.41	0.32
190	0.497	374	78	0.28	0.32	1.170	2.600	163	66	0.40	0.32
200	0.492	327	79	0.31	0.33	1.166	2.568	141	65	0.40	0.33
210	0.487	312	78	0.28	0.34	1.160	2.560	133	65	0.40	0.34
210[a]	0.484	274	82	0.35	0.34	1.159	2.560	116	65	0.40	0.34
212.5[a]	0.484	256	83	0.37	0.34	1.167	2.558	108	65	0.37	0.34
215[a]	0.482	232	81	0.32	0.36	1.158	2.556	98	65	0.35	0.36
217.5[a]	0.486	188	86	0.36	0.38	1.162	2.548	79	65	0.35	0.38
219[a]	0.483	155	82	0.37	0.38	1.145	2.545	62	63	0.35	0.38
220[a]	0.486	113	84	0.36	0.38	1.148	2.500	45	65	0.40	0.38
220	0.461	0				1.145	2.500	0			

[a] Data obtained upon cooling.

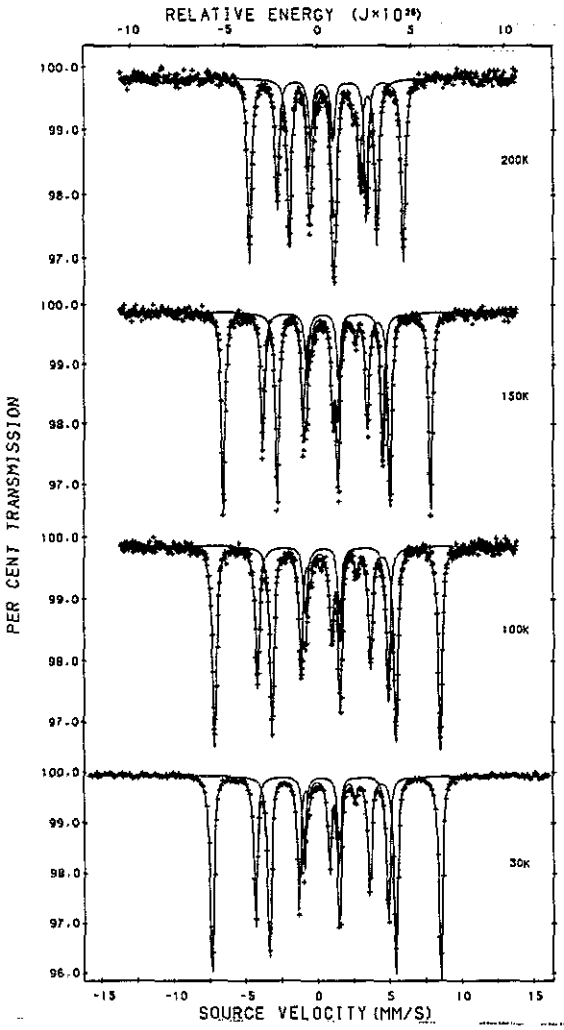

Figure 8. The Mössbauer spectra of α-$Fe_2(PO_4)O$ obtained at several temperatures below its Néel temperature.

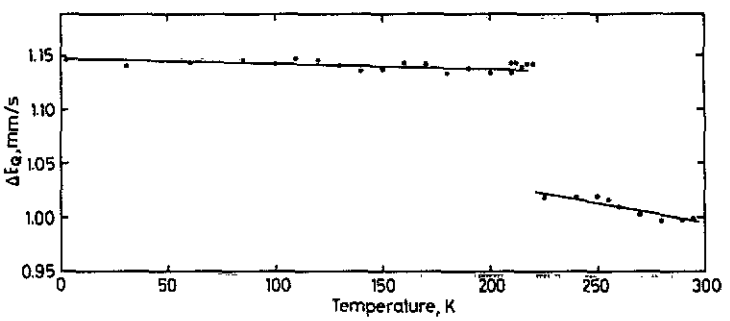

Figure 9. The temperature dependence of the quadrupole interaction for the Fe^{3+} site in α-$Fe_2(PO_4)O$. The full lines are drawn as a guide to the eye.

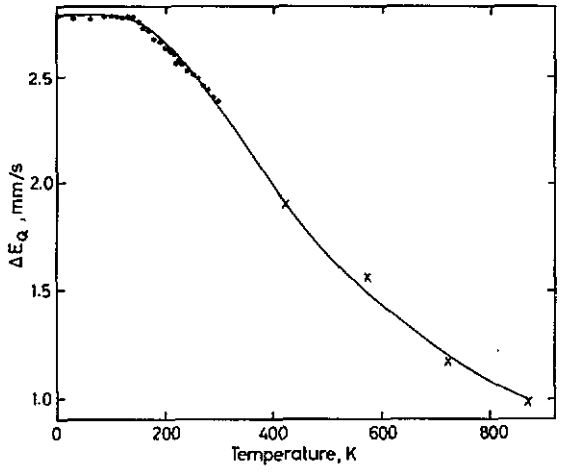

Figure 10. The temperature dependence of the quadrupole interaction for the Fe^{2+} site in α-$Fe_2(PO_4)O$, from 4.2 to 873 K. The × data points are from [2] and the remaining data points are measured in this work. The full curve corresponds to the fit discussed in the text.

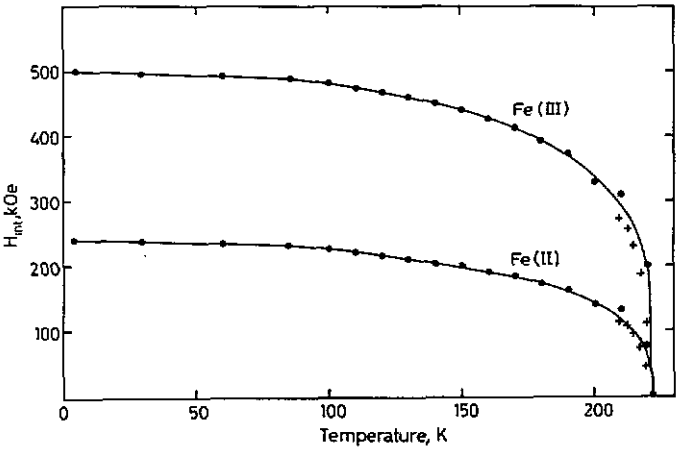

Figure 11. The temperature dependence of the hyperfine fields for the Fe^{2+} and Fe^{3+} sites in α-$Fe_2(PO_4)O$. The + data points were obtained upon cooling and the remaining data points were obtained upon warming of the sample.

indicate that the Néel temperature is between 220.5 and 220 K, a value in good agreement with that obtained from the neutron diffraction results, as is shown in figure 4. The shape of the curves in these two figures is very similar, particularly above 200 K, where the hyperfine fields and the moments collapse very rapidly. The 500 kOe saturation value of the hyperfine field for the Fe^{3+} site is rather lower than would be expected for Fe^{3+} in an ionic lattice [26] and indicates a covalent contribution [27] to the bonding at this site. The 240 kOe saturation value of the hyperfine field for the Fe^{2+} site is in the range measured for Fe^{2+} in the octahedral site of various spinels [26]. The main difference between the plots shown in figures 4 and 11 resides in the rather similar saturation moments and the very different saturation hyperfine fields. This difference occurs because the considerably smaller hyperfine field on Fe^{2+} is due to a non-vanishing orbital

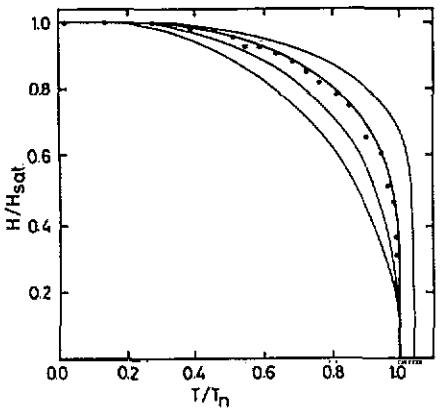

Figure 12. The reduced Fe^{3+} hyperfine field versus the reduced temperature. The full curves are computed as explained in [29] for η values of 0.0, 0.5, 1.0 and 1.5, for the bottom curve to the top curve, respectively. In this figure η is a measure of the departure of the magnetic transition from second order.

moment which produces an additional contribution of opposing sign to the hyperfine field [26, 28].

A plot of the reduced Fe^{3+} hyperfine field versus the reduced temperature, figure 12, shows that the reduced field does not follow a Brillouin curve with $S = 5/2$ but rather follows the curve computed by Bean and Rodbell [29], for $S = 5/2$ and $\eta = 1$, in their treatment of the exchange magnetostriction associated with a non-second-order magnetic transition. The parameter η is a measure of how extensively the transition departs from an ideal second order transition and $\eta = 1$ is at the crossover between first and second order. This η should not be confused with the asymmetry parameter for a quadrupole interaction, which is also traditionally given the symbol η. From the Néel temperature, the relative change of the unit-cell volume at the Néel temperature, the number of atoms in the unit cell, the reduced magnetization at 220 K and η, it is possible, from equations (11) and (12) in [29], to obtain a compressibility, κ, of $2.8\,10^{-10}\,N^{-1}\,m^2$ for α-$Fe_2(PO_4)O$, a value which is relatively large. Unfortunately, there is no experimental value for the compressibility of α-$Fe_2(PO_4)O$. The parameter, β, which measures [29] the slope of the variation of the transition temperature with the lattice volume is found to be +2.4. As might be expected for a non-second-order transition, the Mössbauer spectra measured within a few degrees of the ordering temperature show a small thermal hysteresis in the hyperfine fields, as is shown in figure 11.

The neutron diffraction results discussed above have indicated that the magnetic moments, and hence presumably the hyperfine fields, are oriented along the [010] or *b*-axis in α-$Fe_2(PO_4)O$. Thus, from the value of θ, it should be possible to relate the direction of the principal axis of the electric field gradient tensor to the molecular geometry. For the Fe^{2+} site the vectors to the two Fe^{3+} near-neighbour sites make angles of 62 and 57°; angles which are close to the observed θ value of 66°. There does not seem to be any obvious structural basis for the $80 \pm 2°$ angle found for Fe^{3+}. An angle of 90° would not be unrealistic from the structure but fits with θ constrained to 90° give substantially poorer fits of the magnetic spectra.

In contrast to the fits of the paramagnetic spectra, below the Néel temperature, the areas of the two magnetic components are equal, indicating equivalent recoil-free fractions for the two iron sites. The Mössbauer spectra measured between 85 and 220 K were obtained under fixed geometry conditions with a room temperature source. Hence it is possible to use the temperature dependence of the logarithm of the spectral absorption area and of the isomer shift to obtain information [20, 21, 30] about

the lattice dynamics of α-$Fe_2(PO_4)O$. The slope of the ln area with temperature is $-1.15 \times 10^{-3}\,K^{-1}$. The slopes of the isomer shifts with temperature are $-7.20 \times 10^{-4}\,mm\,s^{-1}\,K^{-1}$ for the Fe^{2+} site and $-6.71 \times 10^{-4}\,mm\,s^{-1}\,K^{-1}$ for the Fe^{3+} site, between 4.2 and 873 K. These slopes yield [21] effective recoiling masses of 58 and 62 g mol^{-1} and lattice Mössbauer temperatures of 342 and 330 K, respectively, for the Fe^{2+} and Fe^{3+} sites.

5. Discussion

In understanding the magnetic properties of α-$Fe_2(PO_4)O$, it is important to consider the magnetic interactions both within and between the ferromagnetic sheets shown in figure 3. Within these sheets, there are numerous pathways for magnetic coupling which include: (1) direct magnetic exchange across the shared octahedral edge between the t_{2g} orbitals on two Fe^{2+} sites; (2) direct magnetic exchange across the shared octahedral face between the t_{2g} orbitals on Fe^{2+} and those on its two Fe^{3+} near neighbours; (3) magnetic superexchange through the 92° Fe^{2+}–O(2)–Fe^{2+} and 103° Fe^{2+}–O(1)–Fe^{2+} exchange pathways; and (4) magnetic superexchange through the 87° Fe^{2+}–O(1)–Fe^{3+}, 82° Fe^{2+}–O(1)–Fe^{3+} and 90° Fe^{2+}–O(4)–Fe^{3+} exchange pathways. Between the sheets, as shown in figure 3, there are two pathways for magnetic coupling: (1) magnetic superexchange through the 119° Fe^{2+}–O(1)–Fe^{3+} exchange pathway; and (2) magnetic superexchange through the 134° Fe^{3+}–O(1)–Fe^{3+} exchange pathway, where both pathways are via O(1). The importance of O(1) in the exchange pathway is also revealed in the Wigner–Seitz cell volume. As expected, all of the Wigner–Seitz cell volumes contract upon cooling, except for that of O(1) which actually expands by ca. 0.1%. Apparently the anti-ferromagnetic exchange between the sheets affects this bridging site more than the remaining oxygen sites. Alternatively, and perhaps more likely, this may indicate that the relative atom positions are different in the paramagnetic and antiferromagnetic phases.

There are numerous additional Fe–O–P–O–Fe superexchange pathways, both within and between the sheets, but they are known to be rather weak [31, 32]. To classify the other magnetic interactions, we can use the rule proposed by Goodenough [33] which indicates that direct exchange and 90° superexchange interactions are weaker than the 180° superexchange interactions. Further, the 180° superexchange interaction is known to increase with the covalency of the metal–oxygen bond, a covalency observed in the Mössbauer effect for the Fe^{3+} site. It is also well known from various spinels [3] that the 134° superexchange interaction is strong and that it becomes stronger as the covalency of the Fe^{3+}–O bond increases. Thus, the antiferromagnetic structure shown in figure 3 results because the antiferromagnetic coupling through the 134° superexchange pathway between sheets predominates. The ferromagnetic coupling within the sheets is expected because both direct exchange and the approximately 90° superexchange between Fe^{2+} and Fe^{2+} or Fe^{3+} are ferromagnetic. Therefore there is no magnetic frustration either within or between the sheets shown in figure 3.

Acknowledgments

The neutron diffraction data were obtained at the Institut Laue Langevin. We are grateful to J L Soubeyroux, responsible for the D1b diffractometer, for his help during

the measurements. The authors thank Dr O A Pringle and Ms M Buhl for their help in obtaining the Mössbauer spectral data and Ms L Gelato for providing the program BLOKJE. The authors also acknowledge with thanks the financial support of NATO for a cooperative scientific research grant (86-0685) and the Petroleum Research Fund administered by the American Chemical Society.

References

[1] Modaressi A, Courtois A, Gérardin R, Malaman B and Gleitzer C 1981 *J. Solid State Chem.* **40** 301
[2] Iraldi R, Le Caër G and Gleitzer C 1981 *Solid State Commun.* **40** 145
[3] Gleitzer C and Goodenough J B 1986 *Structure and Bonding* **61** 1
[4] Eckert H 1987 *Mössbauer Spectroscopy Applied to Inorganic Chemistry* vol. 2, ed G J Long (New York: Plenum) p 125
[5] Ghose S, Hewat A W and Marezio M 1984 *Phys. Chem. Minerals* **11** 67
[6] Ghose S, Tsukimura K and Hatch D M 1989 *Phys. Chem. Minerals* **16** 483
[7] Ech-Chahed B, Jeannot F, Malaman B and Gleitzer C 1988 *J. Solid State Chem.* **74** 47
[8] Ijjaali M, Malaman B, Gleitzer C, Warner J K, Hriljac J A and Cheetham A K 1990 *J. Solid State Chem.* **86** 195
[9] Malaman B, Ech-Chahed B and Gleitzer C 1988 *The Time Domain in Surface and Structural Dynamics* ed G J Long and F Grandjean (Dordrecht: Kluwer Academic) p 335
[10] Long G J and Grandjean F 1990 *Supermagnets, Hard Magnetic Materials* ed G J Long and F Grandjean (Dordrecht: Kluwer Academic) p 355
[11] Gelato L 1981 *J. Appl. Cryst.* **14** 141
[12] Shannon R D and Prewitt C T 1969 *Acta Crystallogr.* B **25** 925
[13] Freeman A J and Declaux J P 1979 *J. Magn. Magn. Mater.* **12** 11
[14] Wolfers P 1990 *J. Appl. Cryst.* **23** 554
[15] Freeman A J and Watson R E 1961 *Acta Crystallogr.* **14** 231
[16] Malaman B, Ijjaali M, Venturini G, Gleitzer C and Soubeyroux J L 1991 *Eur. J. Solid State Inorg. Chem.* **28** 519
[17] Gavoille G, Gleitzer C and Long G J 1987 *Rev. Chim. Minér.* **24** 42
[18] Sherman D M 1985 *Phys. Chem. Minerals* **12** 161
[19] Belov K P 1981 *Magnetic Transitions* (New York: Consultants Bureau)
[20] Kolk B 1984 *Dynamic Properties of Solids* vol 5, ed G K Horton and A A Maradudin (Amsterdam: North-Holland) p 5
[21] Herber R H 1984 *Chemical Mössbauer Spectroscopy* ed R H Herber (New York: Plenum) p 199
[22] Walker L R, Wertheim G K and Jaccarino V 1961 *Phys. Rev. Lett.* **6** 98
[23] Long G J and Gleitzer C 1990 *Hyperfine Interactions* **62** 147
[24] Gérard A and Grandjean F 1971 *Solid State Commun.* **9** 1845
[25] Ingalls R 1964 *Phys. Rev.* A **133** 787
[26] Vandenberghe R E and De Grave E 1989 *Mössbauer Spectroscopy Applied to Inorganic Chemistry* vol 3, ed G J Long and F Grandjean (New York: Plenum) p 59
[27] Sawatzky G A and van der Woude F 1974 *J. Physique Coll.* **34** C6–34
[28] Cranshaw T E and Longworth G 1984 *Mössbauer Spectroscopy Applied to Inorganic Chemistry* vol 1, ed G J Long (New York: Plenum) p 171
[29] Bean C P and Rodbell D S 1962 *Phys. Rev.* **126** 104
[30] Long G J and Grandjean F 1991 *Applications of Analytical Techniques to the Characterization of Materials* ed D L Perry (New York: Plenum) at press
[31] Battle P D, Cheetham A K, Long G J and Longworth G 1982 *Inorg. Chem.* **21** 4223
[32] Mercader R C, Terminiello L, Long G J, Reichel D G, Dickhaus K, Zysler R, Sanchez R and Tovar M 1990 *Phys. Rev.* B **42** 25
[33] Goodenough J B 1963 *Magnetism and the Chemical Bond* (New York: Wiley-Interscience) p 165